Molecular Therapy
Nucleic Acids
Original Article

LncEDCH1 improves mitochondrial function to reduce muscle atrophy by interacting with SERCA2

Bolin Cai,[1,2,5] Manting Ma,[1,2,5] Jing Zhang,[1,2] Zhijun Wang,[1,2] Shaofen Kong,[1,2] Zhen Zhou,[1,2] Ling Lian,[3] Jiannan Zhang,[4] Juan Li,[4] Yajun Wang,[4] Hongmei Li,[1,2] Xiquan Zhang,[1,2] and Qinghua Nie[1,2]

[1]Lingnan Guangdong Laboratory of Modern Agriculture & State Key Laboratory for Conservation and Utilization of Subtropical Agro-bioresources, College of Animal Science, South China Agricultural University, Guangzhou, Guangdong 510642, China; [2]Guangdong Provincial Key Lab of Agro-Animal Genomics and Molecular Breeding, Key Laboratory of Chicken Genetics, Breeding and Reproduction, Ministry of Agriculture, Guangzhou, Guangdong 510642, China; [3]National Engineering Laboratory for Animal Breeding and MOA Key Laboratory of Animal Genetics and Breeding, College of Animal Science and Technology, China Agricultural University, Beijing 100193, China; [4]Key Laboratory of Bio-Resources and Eco-Environment of Ministry of Education, College of Life Sciences, Sichuan University, Chengdu 610065, China

Skeletal muscle is a regulator of the body's energy expenditure and metabolism. Abnormal regulation of skeletal muscle-specific genes leads to various muscle diseases. Long non-coding RNAs (lncRNAs) have been demonstrated to play important roles in muscle growth and muscle atrophy. To explore the potential function of muscle-associated lncRNA, we analyzed our previous RNA-sequencing data and selected the lncRNA (*LncEDCH1*) as the research object. In this study, we report that *LncEDCH1* is specifically enriched in skeletal muscle, and its transcriptional activity is positively regulated by transcription factor SP1. *LncEDCH1* regulates myoblast proliferation and differentiation *in vitro*. *In vivo*, *LncEDCH1* reduces intramuscular fat deposition, activates slow-twitch muscle phenotype, and inhibits muscle atrophy. Mechanistically, *LncEDCH1* binds to sarcoplasmic/ER calcium ATPase 2 (SERCA2) protein to enhance SERCA2 protein stability and increase SERCA2 activity. Meanwhile, *LncEDCH1* improves mitochondrial efficiency possibly through a SERCA2-mediated activation of the AMPK pathway. Our findings provide a strategy for using *LncEDCH1* as an effective regulator for the treatment of muscle atrophy and energy metabolism.

INTRODUCTION

Skeletal muscle is the largest component in the body representing ~40% of body mass, and is an important regulator of the body's energy expenditure and metabolism.[1–3] Abnormal regulation of skeletal muscle-specific genes leads to various muscle diseases such as sarcopenia, myosarcoma, and muscle metabolic disorder.[4,5]

Muscle hypertrophy and atrophy are two opposing phenomena that are mechanistically linked.[6] Muscle atrophy refers to a decrease in muscle mass and fiber size and is characterized by enhanced protein degradation.[7] By contrast, muscle hypertrophy refers to an increase in muscle mass associated with increased intracellular RNA and protein synthesis and decreased protein degradation, and has been reported to be regulated by many pathways, such as mammalian target of rapamycin (mTOR), insulin-like growth factor, and AMP-activated protein kinase (AMPK) pathways.[8–10] Intracellular calcium ions (Ca^{2+}) are important signaling molecules involved in muscle contraction, secretion, and cell proliferation or death.[11–14] Minor changes in the Ca^{2+} handling apparatus might result in major pathophysiological consequences in the skeletal muscle. Indeed, abnormal expression patterns of ion-regulatory proteins have been repeatedly reported in muscle atrophy.[15–18]

Sarcoplasmic/ER calcium ATPase 2 (SERCA2), located in the ER, is a membrane transport protein that maintains a low cytosolic calcium level to ensure the physiological processes.[19] A decrease in SERCA2 activity causes ER stress, which induces muscular dystrophies via mitochondrial dysfunction and generation of reactive oxygen species (ROS).[16] Mitochondria and ER are physically and functionally interconnected to maintain cytosolic calcium homeostasis. In mitochondria, the homeostasis of calcium promotes the production of ATP and enhances the tricarboxylic acid (TCA) cycle. Meanwhile, mitochondrial dysfunction, which is induced by ER stress, can be fed back and further amplify ER stress.[20–22]

Protein-encoding genes only account for a small portion (2%) of the genome, and the remainder is primarily transcribed into non-coding RNAs (ncRNAs).[23] Long non-coding RNAs (lncRNAs) are a new class of regulatory RNAs with a length of more than 200 nt that been found in the cytoplasm and nucleus.[24,25] Recent studies have demonstrated that lncRNAs have regulated multiple biological processes and participate in skeletal muscle development and muscle disorders.[26–31]

Received 5 May 2021; accepted 7 December 2021;
https://doi.org/10.1016/j.omtn.2021.12.004.

[5]These authors contributed equally

Correspondence: Hongmei Li, College of Animal Science, South China Agricultural University, Guangzhou 510642, Guangdong, China.
E-mail: hongmeili@scau.edu.cn
Correspondence: Qinghua Nie, College of Animal Science, South China Agricultural University, Guangzhou 510642, Guangdong, China.
E-mail: nqinghua@scau.edu.cn

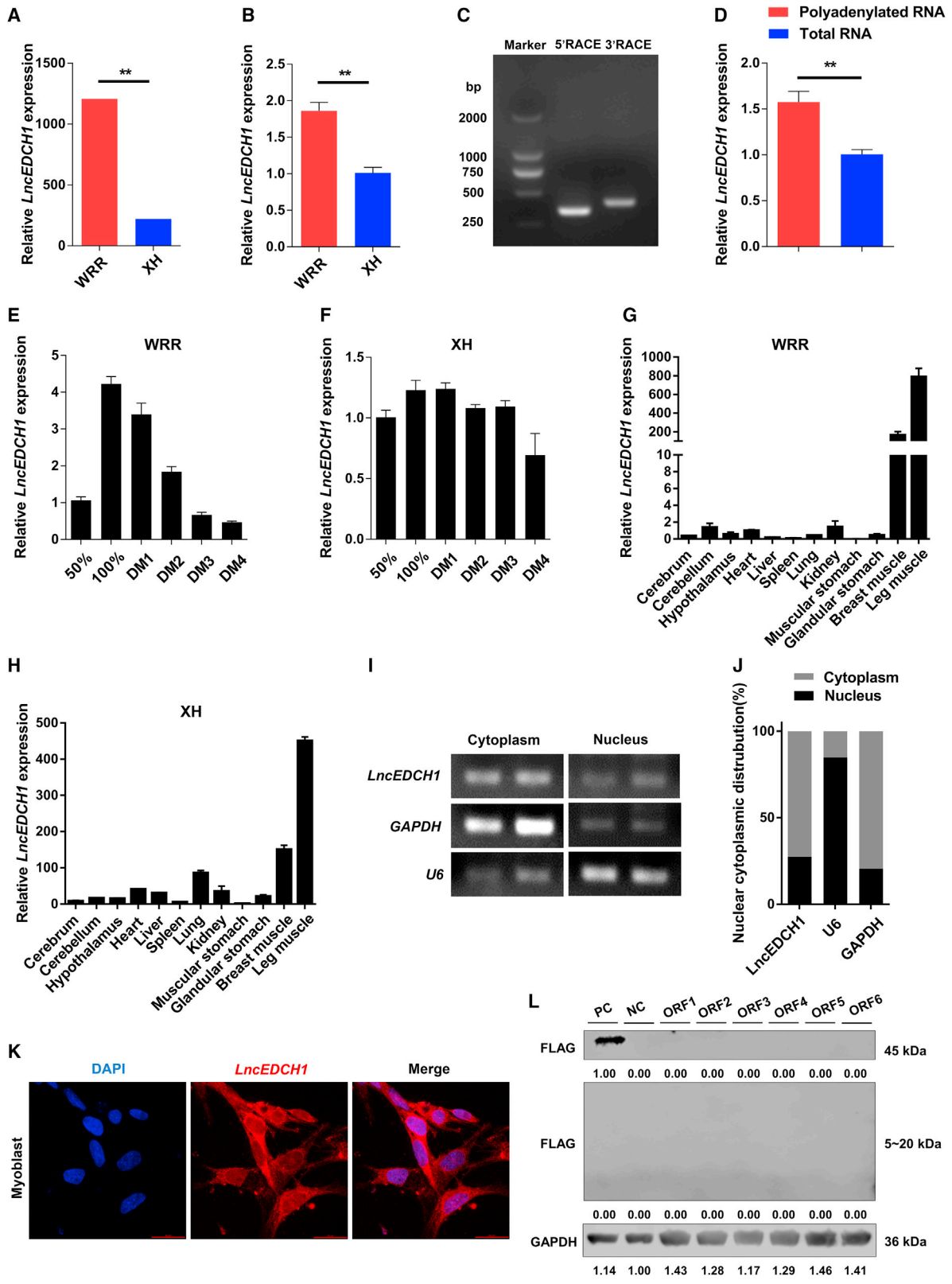

(legend on next page)

In our previous RNA-sequencing (RNA-seq) analysis (accession number GEO: GSE58755), we screened out an lncRNA (TCONS_00059312, generated by epidermal differentiation protein containing cysteine histidine motifs 1 [*EDCH1*] gene, named *LncEDCH1*) differentially expressed in White recessive rock (a fast-growth-rate broiler chicken) and Xinghua chicken (a slow-growth-rate Chinese native breed).[32] In this study, we found that *LncEDCH1* promotes the proliferation of myoblasts and inhibits myogenic differentiation, as well as reducing fat deposition, activating slow-twitch muscle phenotype, and alleviating muscle atrophy by activating the AMPK pathway and ameliorating mitochondrial efficiency. Further research found that *LncEDCH1* exerts its function by maintaining SERCA2 protein stability to increase SERCA2 activity. Our studies uncover a functional lncRNA whereby *LncEDCH1* may be a regulatory molecule for muscle disorders associated with calcium homeostasis.

RESULTS

LncEDCH1 is a muscle-associated lncRNA that is positively regulated by transcription factor SP1

To discover the potential function of muscle-associated lncRNA, we analyzed our previous RNA-seq data and found an lncRNA (*LncEDCH1*) highly expressed in hypertrophic broilers (Figures 1A and 1B).[32] Rapid amplification of cDNA ends (RACE) was performed to identify the 5′ and 3′ ends of *LncEDCH1* (Figure 1C). The Basic Local Alignment Search Tool (BLAST) of the National Center for Biotechnology Information (NCBI) showed that *LncEDCH1* was 590 nt long, located at chromosome 25 from position 3,294,274 to 3,294,232, and 3,293,823 to 3,293,488, relatively conserved in *Meleagris gallopavo* and *Numida meleagris* (Table S1 and Figure S1). *LncEDCH1* was highly expressed in polyadenylated RNA, demonstrating that *LncEDCH1* is a polyadenylated lncRNA (Figure 1D). Moreover, *LncEDCH1* gradually decreased with the myogenic differentiation, and was enriched in breast and leg muscles (Figures 1E–1H). Cell-fractionation assays demonstrated that *LncEDCH1* is mainly present in the cytoplasm of chicken primary myoblasts (CPMs) (Figures 1I and 1J). A similar result was also confirmed by *in situ* RNA hybridization (Figure 1K). To further verify the coding potential of *LncEDCH1*, we cloned 3xFLAG epitope tag in-frame with the C terminus of six potential open reading frames (ORFs) of *LncEDCH1*. Subsequently, western blotting showed that *LncEDCH1* is a non-coding RNA without protein-encoding potential (Figure 1L).

To explore the mechanisms through which *LncEDCH1* is regulated at the transcriptional level, we conducted luciferase assays with four reporter constructs containing different fragments of the *LncEDCH1* promoter (located between −1,931 and +1 bp) (Figure S2A). The region between −1,931 and −1,591 bp had the highest transcriptional activity, which suggests that this region is the core promoter of *LncEDCH1* (Figure S1A). Furthermore, we predicted the transcription factors involved in regulating the transcriptional activity of *LncEDCH1* by bioinformatics analysis, and found that transcription factor SP1 specifically binds to the core promoter region (−1,923 to −1,912 bp) of *LncEDCH1* (Figure S2B). Compared with the mutated constructs, overexpression of *SP1* increased the luciferase activity of reporter constructs containing predicted SP1 binding sites (−1,931 to −1,591 bp) (Figure S2C). At the same time, *SP1* overexpression significantly increased the expression of endogenous *LncEDCH1* (Figure S2D). Collectively, these data revealed that *LncEDCH1* is positively regulated by the transcription factor SP1.

LncEDCH1 promotes proliferation and inhibits differentiation of myoblasts

Given that *LncEDCH1* was upregulated during myoblast proliferation (Figures 1E and 1F), we performed inhibition and overexpression experiments to assess its effect in proliferation and differentiation of myoblasts. *LncEDCH1* was successfully knocked down or overexpressed in CPMs (Figures 2A and S3A), as shown by the results of quantitative PCR (qPCR). Inhibition of *LncEDCH1* reduced cell-cycle-promoting genes such as *PCNA* while increasing the expression of cell-cycle-inhibiting genes (such as *CDKN1A* and *CDKN1B*) (Figure 2B). However, the opposite result was observed with *LncEDCH1* overexpression (Figure S3B). 5-Ethynyl-2′-deoxyuridine (EdU) and cell counting kit-8 (CCK-8) assays showed that interference of *LncEDCH1* decreases EdU incorporation and represses myoblast viability, whereas its overexpression promotes myoblast proliferation (Figures 2C–2E and S3C–S3E). Moreover, flow cytometric analysis revealed that *LncEDCH1* inhibition increases the number of cells that progressed to G_0/G_1 and reduces the number of S-phase cells. Conversely, *LncEDCH1* overexpression resulted in a fewer number of G_0/G_1 and greater number of S-phase cells (Figures 2F and S3F).

To further investigate the role played by *LncEDCH1* in myoblast differentiation, we performed immunofluorescence staining. *LncEDCH1* interference significantly facilitated myoblast differentiation and

Figure 1. Identification of *LncEDCH1*

(A and B) Relative *LncEDCH1* expression in breast muscles of 7-week-old Xinghua (XH) chicken and White recessive rock (WRR) detected by RNA-seq (A) (n = 1) and real-time qPCR (B) (n = 4). (C) Results of *LncEDCH1* 5′ RACE and 3′ RACE. (D) Relative *LncEDCH1* expression in polyadenylated RNA and total RNA (n = 4). (E and F) Relative *LncEDCH1* expression during the proliferation and differentiation of chicken primary myoblasts (CPMs) isolated from WRR (E) (n = 4) and XH chicken (F) (n = 4). (G and H) Tissue expression profiles of *LncEDCH1* in 7-week-old WRR (G) (n = 4) and XH chicken (H) (n = 4). The horizontal axis and vertical axis indicate different tissues and their relative expression values, respectively. (I and J) The distribution of *LncEDCH1* in the cytoplasm and nuclei of CPMs was determined by qPCR (I) (n = 2) and semi-quantitative PCR (J) (n = 4). *GAPDH* and *U6* served as cytoplasmic and nuclear localization controls, respectively. (K) RNA *in situ* hybridization of *LncEDCH1* in CPM Special FISH probes against *LncEDCH1* were modified by Cy3 (red). The nucleus was stained by DAPI (blue). (L) Western blot analysis of the coding ability of *LncEDCH1* (n = 1). The potential ORFs of *LncEDCH1* were cloned into the pcDNA3.1-3xFLAG-C vector. CPMs transfected with β-actin-3xFLAG were used as a positive control (PC) and untransfected CPMs were used as a negative control (NC). In (L), the numbers shown below the bands are folds of band intensities relative to control. Band intensities were quantified by ImageJ and normalized to GAPDH. Data are expressed as a fold change relative to the control. Results are presented as mean ± SEM. In (A), (B), and (D), the statistical significance of differences between means was assessed using an independent-sample t test (**$p < 0.01$).

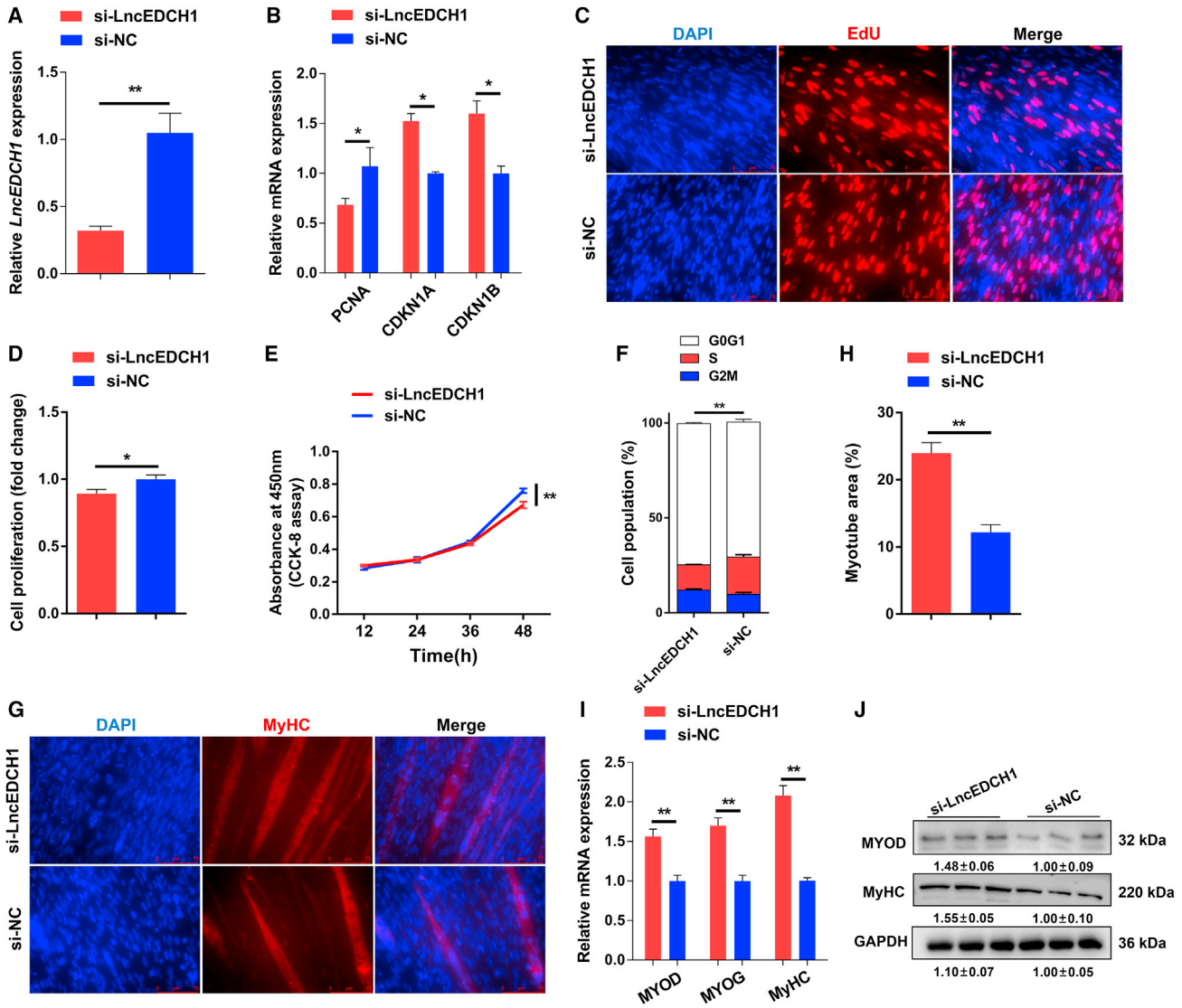

Figure 2. *LncEDCH1* interference suppresses myoblast proliferation but facilitates myogenic differentiation

(A) Relative *LncEDCH1* expression with *LncEDCH1* interference *in vitro* (n = 6). (B) Relative mRNA levels of several cell cycle genes with *LncEDCH1* interference (n = 6). (C) The proliferation of transfected CPMs was assessed by 5-ethynyl-2′-deoxyuridine (EdU) incorporation (n = 3). (D) Proliferation rate of myoblasts after the interference of *LncEDCH1* (n = 3). (E) CCK-8 assays were performed in CPMs with *LncEDCH1* interference (n = 6). (F) Cell cycle analysis of myoblasts after the interference of *LncEDCH1* (n = 4). (G and H) MyHC immunostaining (G) (n = 3) and myotube area (%) (H) (n = 3) of CPMs transfected with *LncEDCH1* interference. Cells were differentiated for 72 h after transfection. (I and J) Relative mRNA (I) (n = 6) and protein (J) (n = 3) expression levels of myoblast differentiation marker genes with *LncEDCH1* interference. In (J), the numbers shown below the bands are folds of band intensities relative to control. Band intensities were quantified by ImageJ and normalized to GAPDH. Data are expressed as a fold change relative to the control. Results are shown as mean ± SEM. In (A), (B), (D–F), (H), and (I), the statistical significance of differences between means was assessed using an independent-sample t test (*$p < 0.05$; **$p < 0.01$).

increased the total areas of myotubes (Figures 2G and 2H). Moreover, the results of qPCR and western blotting showed that expressions of myoblast differentiation marker genes (such as *MYOD*, *MYOG*, and *MyHC*) were upregulated with *LncEDCH1* inhibition (Figures 2I and 2J). In contrast, *LncEDCH1* overexpression repressed myoblast differentiation and downregulated the expression of myoblast differentiation marker genes (Figures S3G–S3J). Taken together, these data indicated that *LncEDCH1* promotes myoblast proliferation and suppresses myoblast differentiation.

LncEDCH1 accelerates fatty acid oxidation, reduces lipid deposition, and promotes TCA cycle in skeletal muscle

To verify whether *LncEDCH1* is involved in the development of skeletal muscle *in vivo*, we injected the gastrocnemius muscle of 1-day-old

chicks with lentivirus-mediated *LncEDCH1* knockdown (Lv-shLncEDCH1) or lentivirus-mediated *LncEDCH1* overexpression (Lv-LncEDCH1) (Figures 3A and S3A). *LncEDCH1* knockdown significantly reduced mitochondrial content, inhibited the fatty acid oxidation (FAO) rate, and facilitated the accumulation of free fatty acid (FFA) and triglyceride (TG), while its overexpression increased mitochondrial content and promoted FAO (Figures 3B–3D and S4B–S4D). Meanwhile, knockdown of *LncEDCH1* downregulated FAO-related genes such as *CPT1* and mitochondrial content regulators such as *PGC1α*, as well as upregulating key genes involved in fatty acid synthesis (such as *FASN* and *ACC*) (Figures 3E and 3F). In contrast, overexpression of *LncEDCH1* showed opposite results (Figures S4E and S4F), indicating that *LncEDCH1* promotes FAO and inhibits lipid deposition.

Mitochondria are the central energy producers in cells due to their ability to generate numerous ATP from metabolizing fatty acids and the glycolytic product pyruvate through the TCA cycle.[33,34] Given that knockdown of *LncEDCH1* reduced the content of mitochondria (Figure 3B), we further performed a central carbon metabolic profiling to study the regulation of *LncEDCH1* on skeletal muscle metabolism. The result of hierarchical clustering analysis (HCA) clearly separated controls and *LncEDCH1* knockdown (Figure 3G and Table S2). For example, compared with control, glycolytic metabolites such as glucose 6-phosphate and fructose 6-phosphate were significantly increased with *LncEDCH1* knockdown (Figure 3H and Table S2). In the meantime, metabolites of the TCA cycle, including citric acid and *cis*-aconitic acid, were significantly reduced (Figure 3H and Table S2). Altogether, our results indicated that *LncEDCH1* decreases the end products of glycolysis and elevates metabolites of the TCA cycle by promoting mitochondrial function, leading to reduction of lipid metabolites (Figure 3I).

LncEDCH1 induces slow-twitch muscle phenotype and inhibits muscle atrophy

The occurrence and transformation of myofiber types are regulated by a variety of factors, which are closely related to the mechanism of muscle metabolism.[35–37] Recent studies have found that skeletal muscle can be remodeled by activating signaling pathways to reprogram gene expression and sustain muscle performance.[38] Compared with glycolytic myofibers (fast-twitch), the oxidative (slow-twitch) myofibers have more myoglobin and mitochondria, as well as higher activity of oxidative metabolic enzymes.[39,40] Given that *LncEDCH1* mediated the flux of glycolysis and TCA cycle (Figure 3I), we speculate that *LncEDCH1* may function in the transformation of myofiber type by regulating muscle metabolism. *LncEDCH1* knockdown reduced the content of glycogen and ATP in gastrocnemius, whereas its overexpression promoted the accumulation of glycogen and ATP (Figures 4A, 4B, S5A, and S5B). Moreover, knockdown of *LncEDCH1* enhanced the activity of lactic dehydrogenase (LDH) and suppressed the activity of succinate dehydrogenase (SDH) (Figure 4C). On the contrary, *LncEDCH1* overexpression decreased glycolytic capacity and elevated oxidative capacity of skeletal muscle (Figure S5C). The expression levels of glycogenolytic and glycolytic genes (such as *HK1*, *PGAM1*, *PYGL*, and *PGK1*) were further tested, whereby it was found that knockdown of *LncEDCH1* upregulated glycogenolytic and glycolytic genes (Figure 4D). Contrastingly, opposite results were shown with *LncEDCH1* overexpression (Figure S5D), suggesting that *LncEDCH1* impeded the glycolysis process and repressed skeletal muscle glycolysis. *LncEDCH1* knockdown led to the upregulation of fast-twitch myofiber genes (such as *SOX6*, *TNNC2*, and *TNNT3*) and inhibited the expression of slow-twitch myofiber genes such as *TNNC1* and *TNNT1* (Figure 4E). More importantly, the results of immunohistochemistry showed that *LncEDCH1* knockdown promoted the expression level of MYH1A/fast-twitch protein and suppressed the expression level of MYH7B/slow-twitch protein (Figures 4F and 4G). By contrast, overexpression of *LncEDCH1* improved the expression of slow-twitch myofiber genes and slow-twitch protein level, and drove the transformation of fast-twitch to slow-twitch myofibers (Figures S5E–S5G).

Numerous studies have found that glycolytic myofibers are more susceptible to atrophy compared with the oxidative myofibers.[41,42] There was a significant decrease in muscle mass and mean cross-sectional area (CSA) with *LncEDCH1* knockdown in gastrocnemius, while the opposite result occurred upon *LncEDCH1* overexpression (Figures 4H–4J and S5H–S5J), suggesting that *LncEDCH1* is involved in muscle atrophy. Balanced autophagy flux in skeletal muscle is critical for the overall health of an organism. Maintaining basal autophagy flux is essential to clear damaged organelles or recycle macromolecules in muscles during metabolic stress.[43] mTOR is a master growth regulator that senses and integrates diverse nutritional and environmental cues and has been reported to modulate autophagy flux.[44,45] To further explore the regulatory mechanism of *LncEDCH1* in reducing muscle atrophy, we tested the mTOR-mediated autophagy pathway. *LncEDCH1* knockdown upregulated the expression level of *SQSTM1*, whereas it suppressed autophagy-related genes such as *ULK1* and *MAP1LC3B* (Figure 4K). In the meantime, the phosphorylation level of mTOR was promoted and accompanied by a decrease in LC3BII content with *LncEDCH1* knockdown in gastrocnemius (Figure 4L). Conversely, *LncEDCH1* overexpression inhibited mTOR signaling and activated autophagy (Figures S5K and S5L), suggesting that *LncEDCH1* may alleviate muscle atrophy by increasing basal autophagy flux.

LncEDCH1 interacts with SERCA2 protein to enhance SERCA2 activity

To explore the molecular mechanism of *LncEDCH1* function in skeletal muscle development, we performed RNA pull-down coupled with mass spectrometry to identify its endogenous binding proteins. A total of 282 proteins were found to specifically bind to *LncEDCH1* (Table S3). Gene ontology (GO) and Kyoto Encyclopedia of Genes and Genomes (KEGG) enrichment analysis of these RNA-binding proteins revealed that they are mainly involved in metabolic pathways, calcium signaling pathways, and carbon metabolism (Figures S6A and S6B). Among these, SERCA2, which was previously reported to be involved in mitochondrial metabolism and muscle development in skeletal muscle,[14,46–48] was identified specifically

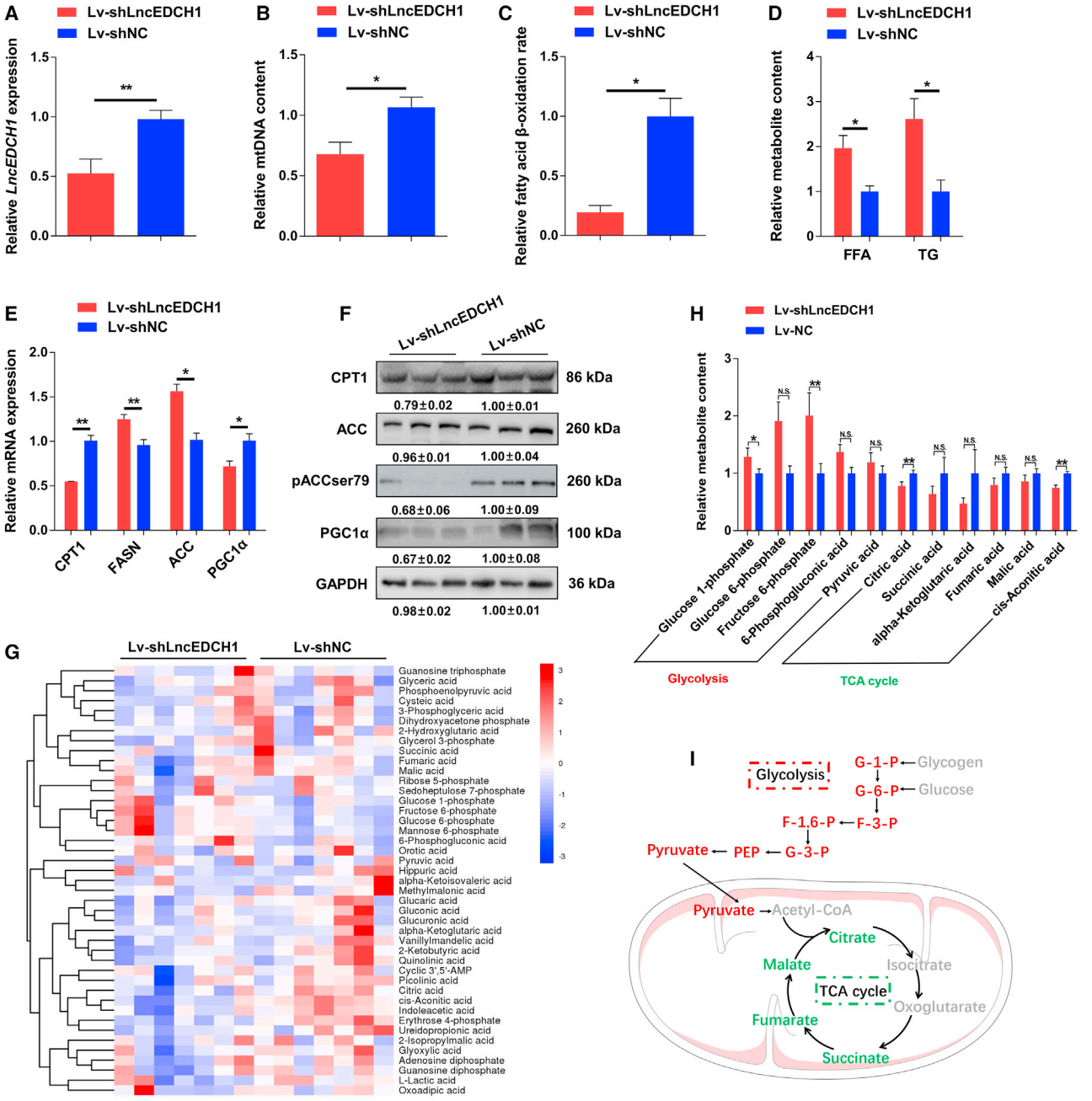

Figure 3. *LncEDCH1* knockdown restrains fatty acid oxidation and tricarboxylic acid cycle in skeletal muscle

(A) Relative *LncEDCH1* expression in gastrocnemius after infection with lentivirus-mediated *LncEDCH1* knockdown (Lv-shLncEDCH1) or negative control (Lv-shNC) (n = 6). (B) Relative mtDNA content in *LncEDCH1* knockdown gastrocnemius (n = 4). (C) Relative fatty acid β-oxidation rate with *LncEDCH1* interference in gastrocnemius (n = 4). (D) Relative free fatty acid (FFA) and triglyceride (TG) content in gastrocnemius with *LncEDCH1* knockdown (n = 4). (E and F) Relative mRNA (E) (n = 4) and protein (F) (n = 3) expression levels of fatty acid oxidation or synthesis-related genes in gastrocnemius with *LncEDCH1* interference. (G) Hierarchical clustering analysis of metabolites in gastrocnemius with interference *LncEDCH1* (n = 7). The colors indicate the relative levels in the *LncEDCH1* knockdown or control group. (H) Relative metabolite content of glycolysis and tricarboxylic acid (TCA) cycle in gastrocnemius with *LncEDCH1* knockdown (n = 7). (I) Schematic diagram of metabolic pathways of glycolysis and TCA cycle affected by *LncEDCH1* knockdown in the gastrocnemius. Upregulated metabolites are shown in red and the downregulated metabolites are shown in green. In (F), the numbers shown below the bands are folds of band intensities relative to control. Band intensities were quantified by ImageJ and normalized to GAPDH. Data are expressed as fold change relative to the control. Results are shown as mean ± SEM. In (A–E) and (H), the statistical significance of differences between means was assessed using paired t tests (*$p < 0.05$; **$p < 0.01$; N.S., no significant difference).

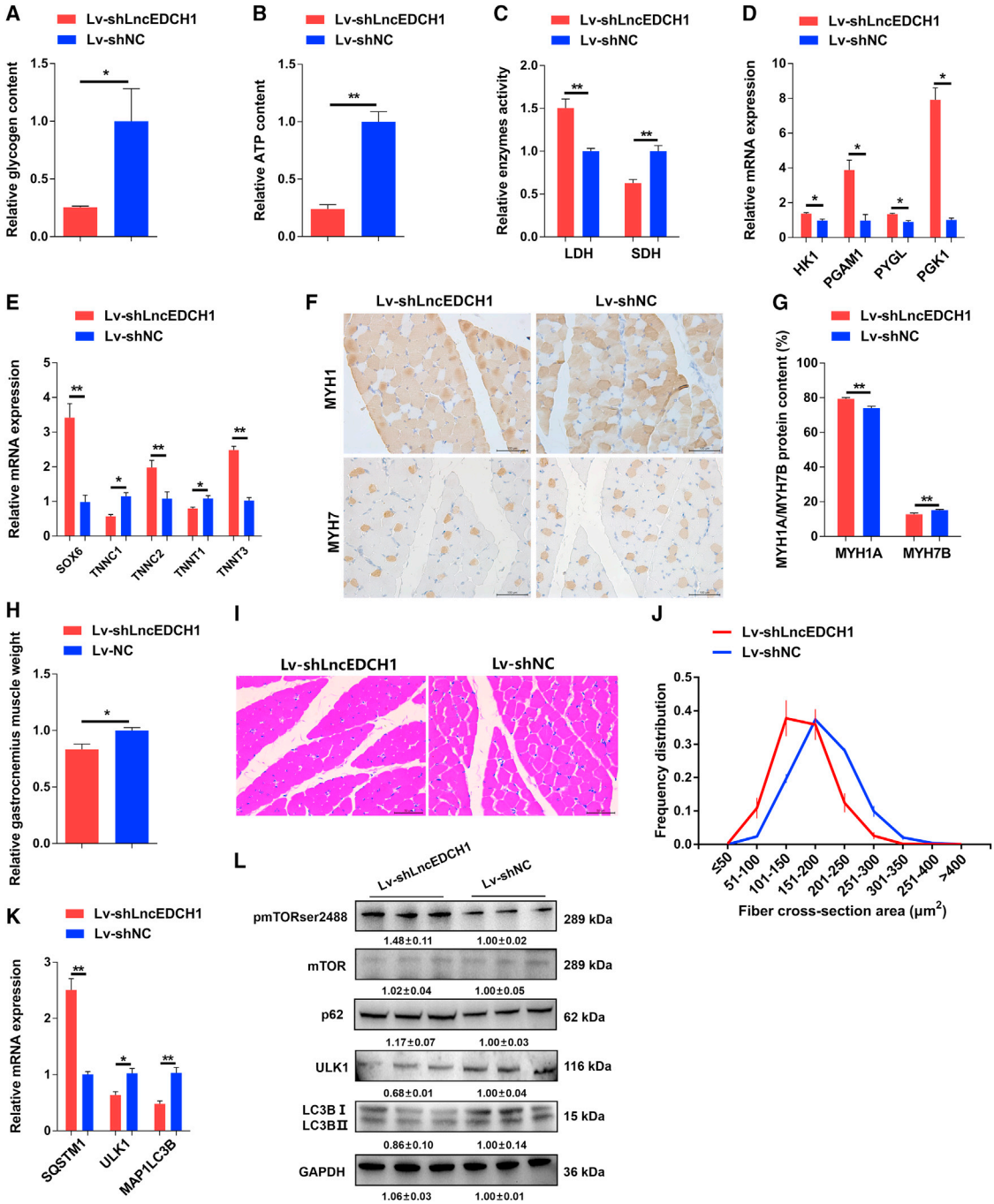

Figure 4. Knockdown of *LncEDCH1* activates fast-twitch muscle phenotype and induces muscle atrophy

(A) Relative glycogen content in *LncEDCH1* knockdown gastrocnemius (n = 4). (B) Relative ATP content in gastrocnemius with *LncEDCH1* interference (n = 4). (C) Relative enzyme activity of lactic dehydrogenase (LDH) and succinate dehydrogenase (SDH) in gastrocnemius infected with *LncEDCH1* knockdown (n = 4). (D) Relative mRNA expression levels of glycogenolytic and glycolytic genes in *LncEDCH1* knockdown gastrocnemius (n = 4). (E) Relative mRNA expression levels of several fast-/slow-twitch myofiber genes in *LncEDCH1* knockdown gastrocnemius (n = 4). (F and G) Immunohistochemistry analysis of MYH1/MYH7 (F) (n = 4) and MYH1/MYH7 protein content (G) (n = 4) in gastrocnemius with knockdown of *LncEDCH1*. (H) Relative gastrocnemius muscle weight after infection with lentivirus-mediated *LncEDCH1* knockdown (n = 6). (I and J) H&E staining (I) (n = 4) and frequency distribution of fiber CSA (J) (n = 4) in *LncEDCH1* knockdown gastrocnemius. (K and L) Relative mRNA expression of autophagy-related genes (K) (n = 6) and the protein (L) (n = 3) expression levels of mTOR signaling in gastrocnemius with *LncEDCH1* interference. In (L), the numbers shown below the bands are folds of band intensities relative to control. Band intensities were quantified by ImageJ and normalized to GAPDH. Data are expressed as fold change relative to the control. Results are shown as mean ± SEM. In (A–E), (G–H), and (K), the statistical significance of differences between means was assessed using paired t tests (*$p < 0.05$; **$p < 0.01$).

bind to *LncEDCH1* (Table S3). To further corroborate this result, we performed RNA immunoprecipitation (RIP) and verified the interaction between *LncEDCH1* and SERCA2 protein (Figure 5A). To determine the functional motifs of *LncEDCH1* corresponding to SERCA2 binding, we constructed a series of truncated *LncEDCH1* fragments. However, unlike the full-length *LncEDCH1*, none of the truncated fragments could physically bind to SERCA2 (Figures 5B and 5C), suggesting that the complete RNA structure is essential for the molecular function of *LncEDCH1*. This interaction of *LncEDCH1* and SERCA2 was also confirmed by their same subcellular distribution pattern as shown by *in situ* RNA hybridization and SERCA2 immunofluorescence staining (Figure 5D).

With the observation that *LncEDCH1* directly interacts with SERCA2 protein, we further analyzed the effect of *LncEDCH1* on *SERCA2*. Overexpression and knockdown of *LncEDCH1* did not change the mRNA expression level of *SERCA2* both *in vivo* and *in vitro* (Figures S7A–S7D). The protein expression level and activity of SERCA2 were increased with *LncEDCH1* overexpression, while *LncEDCH1* knockdown suppressed SERCA2 protein expression and SERCA2 activity (Figures 5E–5L). Meanwhile, rescue experiments, which were performed by *LncEDCH1* interference and *SERCA2* overexpression, reduced suppression of SERCA2 activity (Figure 5M). Considering that *LncEDCH1* regulated SERCA2 protein expression and activity, but did not affect *SERCA2* mRNA level, we speculated that *LncEDCH1* may be involved in the regulation of SERCA2 protein stability. Cycloheximide (CHX) is a bacterial toxin that can inhibit protein biosynthesis. Treatment with CHX decreased the expression of SERCA2 protein (Figure 5N). More importantly, overexpression of *LncEDCH1* relieved the decline of SERCA2 protein expression induced by CHX (Figure 5N), implying that *LncEDCH1* interacts with SERCA2 protein to maintain SERCA2 protein stability and increase SERCA2 activity.

LncEDCH1 regulates Ca^{2+} homeostasis and activates the AMPK pathway to improve mitochondrial efficiency

As the sarcoplasmic/ER calcium ATPase, SERCA2 was well known to regulate calcium transport from cytosol to ER to maintain Ca^{2+} homeostasis.[19] Given that *LncEDCH1* interacts with SERCA2 protein to enhance SERCA2 activity, we conducted several experiments to evaluate the effect of *LncEDCH1* on Ca^{2+} homeostasis. Fluo-8-AM, a calcium indicator, was used to investigate the changes of free Ca^{2+} concentration intracellularly. Changes in cytosolic calcium were recorded when calcium transport from cytosol to ER was blocked by thapsigargin, a SERCA inhibitor. The amplitude of peak Ca^{2+} transient was calculated according to the equation $(F - F_0)/F_0$, where F represents the maximum value of a Ca^{2+} transient and F_0 represents Ca^{2+} level immediately before the onset of a Ca^{2+} transient. *LncEDCH1* interference reduced the maximum intensity of Fluo-8-AM and the area of the intensity change curve after treatment with 20 μM thapsigargin (Figures 6A–6C). Conversely, overexpression of *LncEDCH1* increased ER calcium levels (Figures S8A–S8C). Ionomycin can cause calcium release from most intracellular stores and is an effective calcium ionophore. Meanwhile, results similar to those upon thapsigargin treatment were observed with the addition of 10 μM ionomycin (Figures 6D–6F and S8D–S8F). Next, the basal cytosolic calcium concentration was measured by using Fura-2 AM. Interference of *LncEDCH1* increased the basal cytosolic calcium concentration, whereas cytosolic calcium was reduced with *LncEDCH1* overexpression (Figures 6G and S8G). Furthermore, *SERCA2* overexpression partially alleviated the decrease in ER calcium level caused by *LncEDCH1* interference (Figures 6H–6J), indicating that *LncEDCH1* regulates Ca^{2+} homeostasis by modulating *SERCA2*.

Numerous studies have shown that mitochondria and ER are physically and functionally interconnected to maintain the homeostasis of cytosolic calcium.[20,21] ER stress can induce mitochondrial dysfunction, leading to insulin resistance.[22] To investigate the role of *LncEDCH1* in mitochondria, we measured mitochondrial content and function after *LncEDCH1* inhibition and overexpression in CPMs. *LncEDCH1* interference decreased mitochondrial DNA (mtDNA) content accompanied by a decline of mitochondrial membrane potential (Figures 6K and 6L). Meanwhile, ROS production was significantly increased after *LncEDCH1* inhibition (Figure 6M). Inversely, overexpression of *LncEDCH1* upregulated mitochondrial content and enhanced mitochondrial function (Figures S8H–S8J). The activities of mitochondrial electron transport chain (ETC) complexes I, II, and V were repressed after transfection with *LncEDCH1* small interfering RNA (siRNA), whereas overexpression of *LncEDCH1* promoted activities of ETC complexes I, II, and V (Figures 6N–6P and S8K–S6M). In addition, cellular mitochondrial activities including oxygen consumption rate (OCR), basal and maximal mitochondrial respiration, and ATP production were suppressed with *LncEDCH1* inhibition (Figures 6Q and 6R). Meanwhile the opposite result was observed with *LncEDCH1* overexpression (Figures S8N and S8O), illustrating that *LncEDCH1* promotes mitochondria biogenesis.

Calcineurin is a calmodulin-dependent, calcium-activated, serine/threonine protein phosphatase that reportedly mediates multiple signaling cascades in response to changes in cellular calcium ions.[49–51] As the main signal pathway regulating mitochondrial biogenesis, the AMPK-dependent pathway has recently been reported to be negatively regulated by calcineurin.[52–54] Given that *LncEDCH1* regulated Ca^{2+} homeostasis and improved mitochondrial efficiency, we further assessed the calcineurin-mediated AMPK pathway. Inhibition of *LncEDCH1* upregulated the protein level of calcineurin, whereas calcineurin was reduced with *LncEDCH1* overexpression (Figures 6S and S8P). Moreover, the phosphorylation of AMPK and cAMP response element-binding protein (CREB) were suppressed after *LncEDCH1* interference, whereas the AMPK/CREB/peroxisome proliferator-activated receptor γ coactivator 1α (PGC-1α) pathway was activated upon *LncEDCH1* overexpression (Figures 3F, 6S, S4F, and S8P), demonstrating that *LncEDCH1* regulates Ca^{2+} homeostasis to activate the AMPK pathway, thereby improving mitochondrial efficiency.

The function of *LncEDCH1* depends on the regulation of SERCA2 to a certain extent

SERCA2 was highly expressed in breast and leg muscle and upregulated during myoblast differentiation (Figures S9A and S9B),

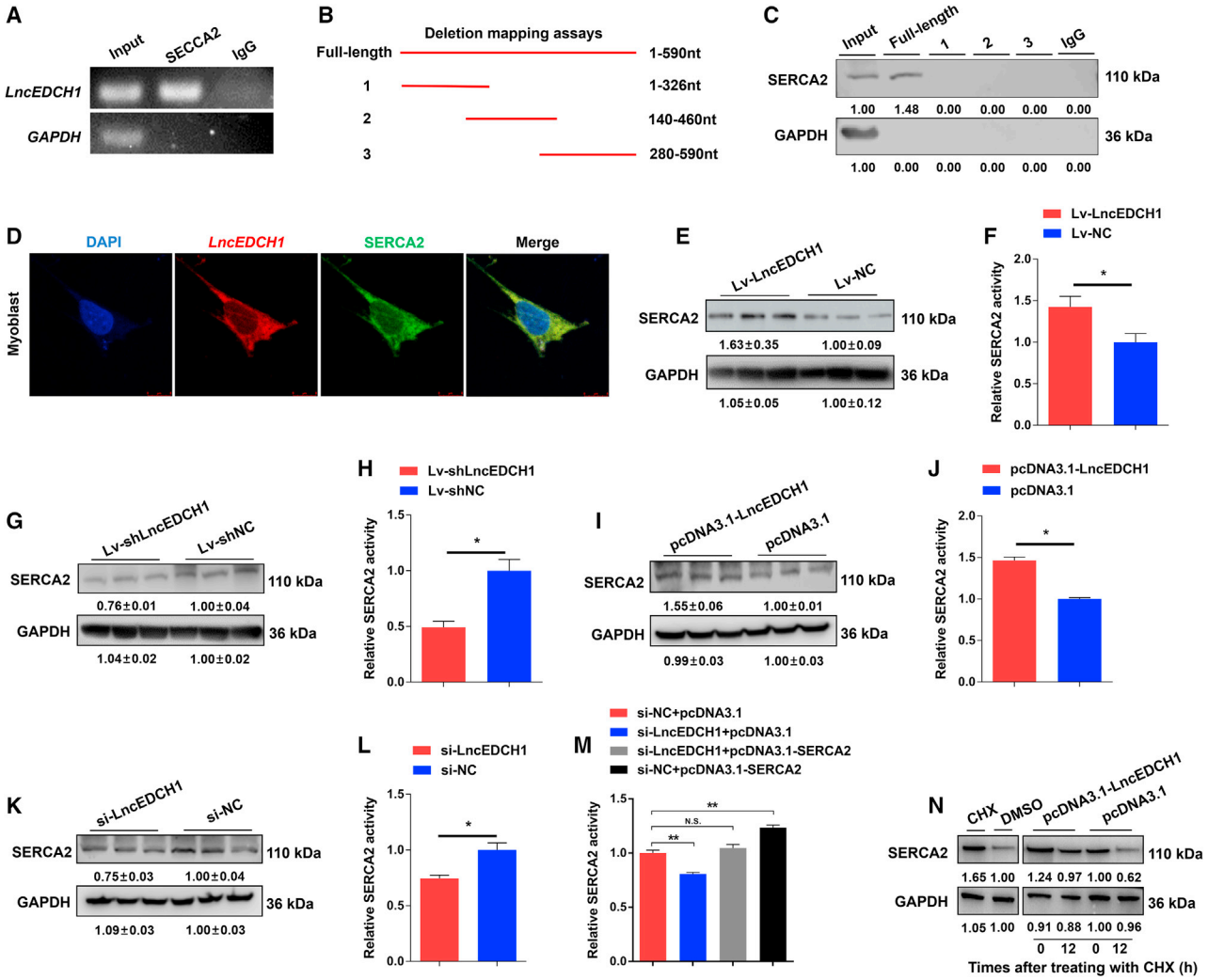

Figure 5. *LncEDCH1* interacts with SERCA2 and enhances Ca^{2+}-ATPase activity

(A) *LncEDCH1* interacts with SERCA2 protein were determined by RNA immunoprecipitation (RIP). (B and C) The interaction of full-length and truncated *LncEDCH1* (base pairs 1–590, 140–460, and 280–590) (B) with SERCA2 protein was determined by RNA pull-down (C). (D) RNA FISH and immunofluorescence staining showed that *LncEDCH1* co-localized with SERCA2 in CPMs. Magnification: 40×. (E–H) Protein expression levels of SERCA2 (E and G) (n = 3) and relative SERCA2 activity (F and H) (n = 4) after *LncEDCH1* overexpression or knockdown *in vitro*. (I–L) Protein expression levels of SERCA2 (I and K) (n = 3) and relative SERCA2 activity (J and L) (n = 4) after *LncEDCH1* overexpression or knockdown *in vivo*. (M) Relative SERCA2 activity induced after co-transfection with the listed nucleic acids in CPMs (n = 3). (N) Protein expression level of SERCA2 in *LncEDCH1* overexpressed myoblast was analyzed after incubation with the protein synthesis inhibitor cycloheximide (CHX; 25 μg/mL) (n = 1). In (C), (E), (G), (I), (K), and (N), the numbers shown below the bands are folds of band intensities relative to control. Band intensities were quantified by ImageJ and normalized to GAPDH. Data are expressed as fold change relative to the control. Results are presented as mean ± SEM. In (F), (H), (J), (L), and (M), the statistical significance of differences between means was assessed using an independent-sample t test (F and H), paired t test (F and H), and ANOVA followed by Dunnett's test (M) (*$p < 0.05$; **$p < 0.01$; N.S., no significant difference).

implying that it may play an important role in skeletal muscle development. Subcellular location annotation showed that SERCA2 protein exists in the ER (Figure S9C), consistent with our results (Figure 5D). To explore the potential biological functions of *SERCA2* in myogenesis, we performed a series of experiments *in vivo*. *SERCA2* overexpressed promoted myoblast proliferation and inhibited myoblast differentiation. On the contrary, interference of *SERCA2* inhibited the proliferation of myoblasts and promoted the differentiation of myoblasts (Figures S10A–S10T), which is similar to *LncEDCH1* in function.

Given the expression and functional relationship between *LncEDCH1* and SERCA2, we further verified the role of *SERCA2* on *LncEDCH1*-mediated skeletal muscle development. Crucially, the regulatory effects of *LncEDCH1* knockdown were weakened after *SERCA2* overexpression (Figures 7A–7H),

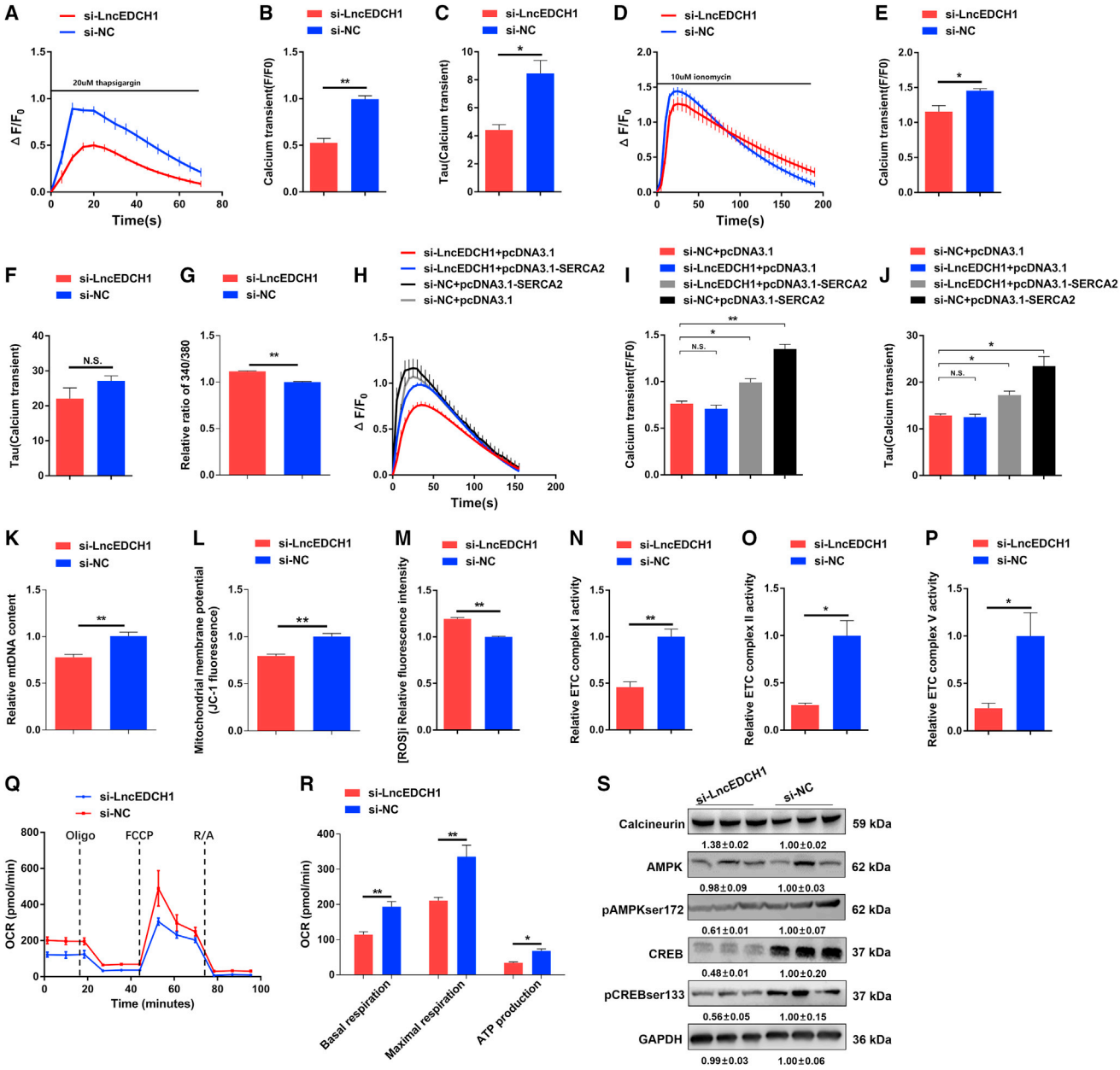

Figure 6. *LncEDCH1* interference destroys Ca^{2+} homeostasis and inactivates the AMPK pathway to reduce mitochondrial efficiency

(A–C) After treatment with 20 μM thapsigargin, change in Fluo-8-AM fluorescence intensity ($F - F_0/F_0$) with time (A) (n = 4), maximum fluorescence intensity in (A) and (B) (n = 4), and areas under the curves (AUC) in (A) and (C) (n = 4) with *LncEDCH1* interference *in vitro*. (D–F) Treatment with 10 μM ionomycin evoked change in Fluo-8-AM fluorescence intensity (D) (n = 4), the maximum fluorescence intensity in (D) and (E) (n = 4), and AUC in (D) and (F) (n = 4) after interference of *LncEDCH1*. (G) Relative basal cytosolic calcium level with *LncEDCH1* interference (n = 6). (H–J) Treatment with 10 μM ionomycin evoked change in Fluo-8-AM fluorescence intensity (H) (n = 3), the maximum fluorescence intensity in (H) and (I) (n = 3), and AUC in (H) and (J) (n = 3) induced after co-transfection with the listed nucleic acids. (K–M) Relative mtDNA content (K) (n = 5), mitochondrial membrane potential (L) (n = 6), and intracellular ROS ([ROS]i) (M) (n = 4) with *LncEDCH1* interference *in vitro*. (N–P) Relative enzyme activity of ETC complexes I (N) (n = 3), II (O) (n = 3), and V (P) (n = 3) with *LncEDCH1* inhibition in CPMs. (Q and R) Oxygen consumption rate (OCR) (Q) (n = 5), and basal respiration, maximal respiration, and ATP production (R) (n = 5) of myoblasts after interference of *LncEDCH1*. (S) Protein expression levels of calcineurin and AMPK signaling after the interference of *LncEDCH1 in vitro* (n = 3). In (S), the numbers shown below the bands are folds of band intensities relative to control. Band intensities were quantified by ImageJ and normalized to GAPDH. Data are expressed as fold change relative to the control. Results are presented as mean ± SEM. In (B), (C), (E–G), (K–P), and (R), the statistical significance of differences between means was assessed using an independent-sample t test. In (I) and (J), ANOVA followed by Dunnett's test was used (*$p < 0.05$; **$p < 0.01$; N.S., no significant difference).

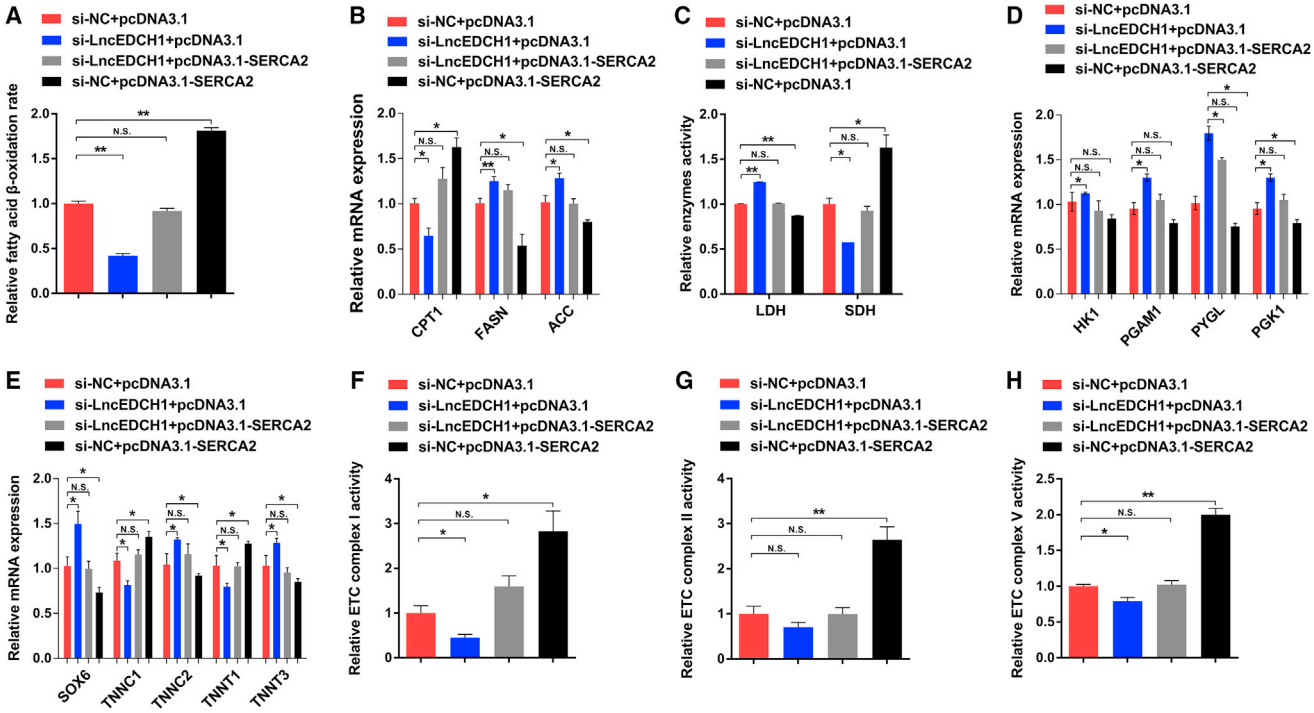

Figure 7. SERCA2 is required for the function of *LncEDCH1*

(A–H) Relative fatty acid β-oxidation rate (A) (n = 3), relative mRNA levels of fatty acid oxidation or synthesis-related genes (B) (n = 3), relative enzyme activity of LDH and SDH (C) (n = 3), relative mRNA expression levels of glycogenolytic and glycolytic genes (D) (n = 3), relative mRNA expression levels of several fast-/slow-twitch myofiber genes (E) (n = 3), and relative enzyme activities of ETC complexes I (F) (n = 3), II (G) (n = 3), and V (H) (n = 3) induced by the listed nucleic acids in CPMs. Results are shown as mean ± SEM. In all panels, the statistical significance of differences between means was assessed using ANOVA followed by Dunnett's test (*$p < 0.05$; **$p < 0.01$; N.S., no significant difference).

hinting that SERCA2 is indispensable to the function of *LncEDCH1*.

DISCUSSION

Myogenesis is a complex process that is finely tuned and controlled by a series of myogenic regulatory factors.[43,55] These factors can regulate myoblasts to withdraw from the cell cycle, express muscle-specific genes, and prevent the expression of other cell- or tissue-specific genes. It is worth noting that recently, lncRNAs have also been demonstrated to function in myogenesis.[31,56,57] *LncEDCH1* is an lncRNA that is differentially expressed between hypertrophic broiler and lean Chinese native breed and was identified by our previous RNA-seq data. In this study, we found that *LncEDCH1* is specifically enriched in skeletal muscle, and its transcriptional activity is positively regulated by transcription factor SP1. Functional studies demonstrated that *LncEDCH1* promoted myoblast proliferation but inhibited myoblast differentiation.

Molecular decoy is one of the main molecular mechanisms for an lncRNA to function. This refers to the fact that lncRNA directly binds to RNA or protein molecules, thereby activating or blocking the role and signal pathway of these molecules.[58] Here, SERCA2, a key ER Ca^{2+}-ATPase that regulates the calcium transport from cytosol to ER, was found to specifically bind to *LncEDCH1*. *LncEDCH1* interacts with SERCA2 to enhance the stability of SERCA2 protein, thus increasing SERCA2 activity and strengthening ER calcium storage.

Skeletal muscle is a major player in regulating glucose uptake, lipid storage, and energy balance, which can maintain systemic energy homeostasis in response to various metabolic stresses.[59] As the main organelle of energy metabolism, mitochondria modulate metabolic processes including TCA cycle, ATP production, and amino acid catabolism, and are closely related to the development of skeletal muscle.[60,61] In the current study, we found that *LncEDCH1* reduced cytosolic calcium to inhibit calcineurin, which causes activation of the AMPK pathway and promotes mitochondrial efficiency.

Autophagy is a highly conserved homeostatic process carrying out degradation of cytoplasmic components including damaged organelles, toxic protein aggregates, and intracellular pathogens.[62] It has come to light that excess autophagy promotes extensive muscle wasting that affects tissue mass, muscle strength, and myofiber regeneration.[63] However, muscle-specific *Atg7* knockout mice have been reported to exhibit muscle loss and dysfunction, hinting that

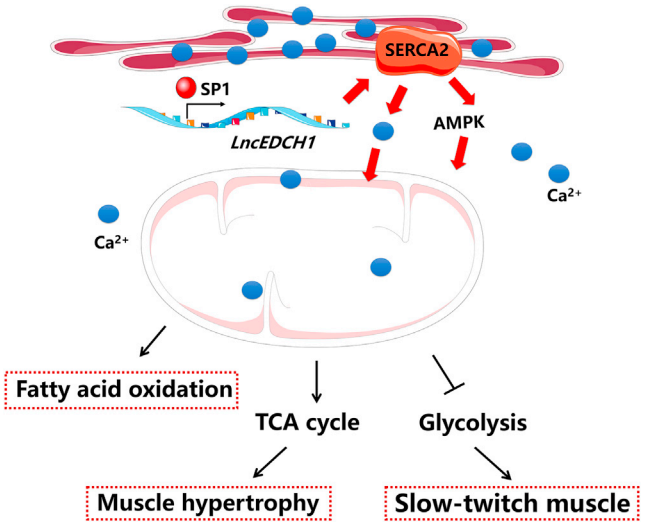

Figure 8. Model of *LncEDCH1* interacts with SERCA2 to improve mitochondrial efficiency, thus promoting intramuscular fatty acid oxidation as well as activating slow-twitch muscle phenotype and inhibiting muscle atrophy.

autophagy is required to maintain muscle mass.[64] Recently, the enhancement of autophagy and the promotion of mitochondrial function have also been found to alleviate muscle atrophy.[65] Here, we found that *LncEDCH1* activated autophagy by inhibiting mTOR signaling. *LncEDCH1* reduces intramuscular fat deposition, as well as activating slow-twitch muscle phenotype and inhibiting muscle atrophy, which potentially lends credence to its function in autophagy and mitochondrial biogenesis.

In conclusion, we demonstrated that *LncEDCH1* can bind with SERCA2 to modulate SERCA2 activity. *LncEDCH1* maintained ER Ca^{2+} homeostasis and improved mitochondrial efficiency to reduce intramuscular fat deposition, activate slow-twitch muscle phenotype, and relieve muscle atrophy (Figure 8). Our study shows that *LncEDCH1* could be an effective regulator for the treatment of energy metabolism and muscle atrophy.

MATERIALS AND METHODS

Animals and ethics statement

Chinese native breeds (XH chickens) were used for the *in vivo* experiment in this study. For construction of animal models of *LncEDCH1* overexpression and knockdown, sample group lentivirus was injected into the left gastrocnemius and control group lentivirus was injected into the right gastrocnemius at a dosage of 1×10^6 IU/mL (at the age of 1, 4, and 8 days). Fourteen days after the initial injection, chick gastrocnemius samples were collected. The use of animals was approved by conformed to "The Instructive Notions with Respect to Caring for Laboratory Animals" issued by the Ministry of Science and Technology of the People's Republic of China, and approved by the Institutional Animal Care and Use Committee at the South China Agricultural University (approval ID: 2020-C036).

Cell culture and transfection

CPMs were isolated from E11 chicken leg muscles as previously described[66] and cultured in Roswell Park Memorial Institute (RPMI)-1640 medium (Gibco, USA) with 20% fetal bovine serum (Gibco).

All transient transfections were performed using Lipofectamine 3000 reagent (Invitrogen, USA) according to the manufacturer's instructions.

RACE

The full-length of *LncEDCH1* was amplified by using a SMARTer RACE cDNA Amplification Kit (Clontech, Japan), following the manufacturer's instructions.

RNA FISH

RNA fluorescence *in situ* hybridization (FISH) experiments were performed using an lncRNA FISH Kit (Guangzhou RiboBio, Guangzhou, China) according to the manufacturer's instructions. In brief, the cells were incubated with the RNA probes in hybridization buffer overnight at 37°C. The cells were washed three times with saline-sodium citrate buffer, stained with 4′,6-diamidino-2-phenylindole (DAPI) for 10 min at room temperature, and examined using a fluorescence microscope.

Luciferase reporter assay

Different fragments of the *LncEDCH1* promoter were cloned into a pGL3-basic luciferase reporter vector (Addgene, USA), and the constructed luciferase reporter vectors were transfected into CPMs in a 96-well plate. The luciferase assay was performed using the Dual-Luciferase Reporter Assay System (Promega, USA) following the manufacturer's instructions.

CCK-8, EdU, and flow cytometry assays

A TransDetect CCK kit (TransGen Biotech, China), an EdU Apollo In Vitro Imaging Kit (RiboBio, China), and a Cell Cycle Analysis Kit (Thermo Fisher Scientific, USA) were used for CCK-8, EdU, and flow cytometry assay, respectively, according to the manufacturers' protocols.

RNA extraction, cDNA synthesis, and real-time qPCR

Total RNA was extracted using TRIzol reagent (TaKaRa, Japan) following the manufacturer's protocol. A PARIS Kit (Ambion, USA) was used to harvest the cytoplasmic and nuclear cell lysates. A PrimeScript RT Reagent Kit with gDNA Eraser (Perfect Real Time) (TaKaRa, Japan) was used to synthesize cDNA. An iTaq Universal SYBR Green Supermix Kit (Toyobo, Japan) was used for cDNA quantification, according to the manufacturer's protocol. All primers for RT-PCR and real-time qPCR are listed in Table S4.

Plasmid construction and RNA oligonucleotides

For FLAG fusion protein construction, six ORFs of *LncEDCH1* were amplified and cloned into the pcDNA3.1-3xFLAG-C vector. For *LncEDCH1* and *SERCA2* overexpression plasmid construction, the full-length sequence *LncEDCH1* and the *SERCA2* coding sequence

were amplified by PCR and cloned into a pcDNA3.1 vector (Promega).

For construction of viral vectors, the full-length sequence of *LncEDCH1* was amplified and then cloned into a pLVX-mCMV-ZsGreen-IRES-Puro vector (Addgene). Short hairpin RNA (shRNA) against *LncEDCH1* was designed by Shanghai Hanbio Biotechnology and subcloned into the pLVX-shRNA2-Puro vector (Addgene).

LncEDCH1 is an lncRNA molecule mainly present in the cytoplasm; the siRNAs that were used for the specific knockdown of *LncEDCH1* and *SERCA2* (NCBI: NM_001271973.1) were designed and synthesized by Guangzhou RiboBio.

Immunofluorescence, immunohistochemistry and hematoxylin and eosin staining

Immunofluorescence was performed using anti-MyHC (B103; DHSB, USA; 2.5 μg/mL), and images were captured using a fluorescence microscope (DMi8; Leica, Germany). The area of cells labeled with anti-MyHC was measured and calculated as previously described.[29]

Immunohistochemistry was carried out using an SP-POD Kit (SP0041; Solarbio, China) with primary antibodies including anti-MYH1(F59, DHSB, 1:100) and anti-MYH7 (S58, DHSB, 1:300).

Hematoxylin and eosin (H&E) staining was performed using muscle tissues embedded in paraffin and cut into 4-μm-thick transverse sections. Subsequently, the sections were stained with H&E.

Western blot analysis

Western blot analysis was performed as previously described.[66] The primary antibodies used were anti-FLAG (AF519, Beyotime, 1:1,000), anti-MYOD (ABP53067, Abbkine, 1:500), anti-MyHC (B103, DHSB, 0.5 μg/mL), anti-SERCA2 (NB100-237, Novus, 1:2,000), anti-ACC (PA5-17564, Thermo Fisher Scientific, 1:1,000), anti-pACCSer80 (orb315750, Biorbyt, 1:500), anti-CPT1 (bs-23779R, Bioss, 1:500), anti-pmTORSer2488 (#5536, CST, 1:1,000), anti-mTOR (bs-1992R, Bioss, 1:500), anti-ULK1 (bs-3602R, Bioss, 1:500), anti-LC3B (NB100-2220, Novus, 2.0 μg/mL), anti-P62 (18420-1-AP, Proteintech, 1:1,000), anti-CREB (bs-0035R, Bioss, 1:500), anti-pCREBSer133 (ab32096, Abcam, 1:5,000), anti-AMPK (bs-1115R, Bioss, 1:500), anti-pAMPKser712 (ABN-PAB12602, Abnova, 1:2,000), anti-Calcineurin (#2614S, CST, 1:1,000), anti-PGC-1α (66369-1-Ig, Proteintech, 1:5,000), and anti-GAPDH (60004-1-Ig, Proteintech, 1:5,000). ProteinFind goat anti-mouse IgG(H+L), HRP conjugate (HS201-01, TransGen, 1:1,000) and ProteinFind goat anti-rabbit IgG(H+L), HRP conjugate (HS101-01, TransGen, 1:500) were used as secondary antibodies.

mtDNA content and FAO rate assay

Total DNA was extracted using a Tissue DNA Kit (D3396, Omega Biotek, USA) following the manufacturer's protocol. The amount of mitochondrial DNA was determined by quantification of cytochrome *c* oxidase subunit II (*COX2*). The nuclear-encoded *β-globin* gene was used as internal control. Primers used in the study can be found in Table S4.

The mitochondria of myoblast and gastrocnemius were isolated using a Cell/Tissue Mitochondria Isolation Kit (C3601/C3606, Beyotime, China) and then subjected to FAO rate assay with a Colorimetric Fatty Acid Oxidation Rate Assay Kit (HL50679, Haling, China), according to the manufacturer's protocol.

Central carbon metabolic profiling

The gastrocnemius samples (n = 7) of *LncEDCH1* knockdown were used for metabolite extraction and then subjected to high-performance ion exchange liquid chromatography (HPIC)-tandem mass spectrometry analysis. The HPIC separation was carried out using a Thermo Scientific Dionex ICS-6000 HPIC System (Thermo Fisher Scientific). An AB SCIEX 6500 QTRAP+ triple quadrupole mass spectrometer (AB Sciex, USA), equipped with electrospray ionization interface, was applied for assay development.

Metabolic HCA was performed using Cluster3.0 software as previously described.[67]

Metabolite and enzyme activities assays

Content of TG, FFA, ATP, and glycogen as well as enzyme activity of LDH and SDH in skeletal muscle were measured using commercially available kits (BC0625, BC0595, BC0305, BC0345, BC0685, BC0955, respectively; Solarbio, China), according to the manufacturer's instructions.

RNA pull-down assay and RIP assay

Biotinylated RNAs were harvested by using a Ribo RNAmax-T7 biotin-labeled transcription kit (RiboBio, China). A Pierce Magnetic RNA-Protein Pull-Down Kit (Thermo Fisher Scientific) was used in RNA-protein pull-down experiments according to the manufacturer's instructions. The eluted products were identified by mass spectrometry with a Q Exactive mass spectrometer (Thermo Fisher) or western blot. Differentially expressed genes were subjected to enrichment analysis of GO functions and KEGG pathways.

RIP was performed using the Magna RIP RNA-Binding Protein Immunoprecipitation Kit (Millipore, USA) according to the manufacturer's instructions. The antibody used for RIP assays was anti-SERCA2 (NB100-237, Novus, 1:50).

SERCA2 activity measurement

The activity of SERCA2 was assessed by a colorimetric ATPase assay kit (A070-4-2, Nanjing Jiancheng Bioengineering Institute, China). Protein concentration was measured by the BCA method (P0012, Beyotime, China). ATPase activity was normalized by protein content.

Intracellular calcium and intracellular Ca^{2+} transient measurement

At 48 h after transfection, the CPMs were incubated with a 5 μM concentration of the acetoxymethyl ester form of Fura 2 (Fura 2-AM,

Beyotime, China) for 30 min at 37°C. The fluorescence emission (510 nm) was detected using a Fluorescence/Multi-Detection Microplate Reader (BioTek, USA) at 340 nm and 380 nm excitation. Data for ratio fluorescence were normalized to the basal fluorescence.

For the ionomycin- and thapsigargin-evoked calcium release assay, the CPMs were incubated with 5 mM Fluo-8 AM (21081, AAT, USA) for 60 min at 37°C in the dark. After washing three times with HL buffer, the HL buffer was replaced by calcium-free HL buffer containing 2 mM EGTA instead of 1.8 mM $CaCl_2$. Thapsigargin (10 μM) (T9033, Sigma, USA) or ionomycin (20 μM) (S1672, Beyotime, China) in calcium-free HL buffer was used to stimulate Ca^{2+} release. Time-lapse images were recorded by a Lycra Live Cell Microscope. The calcium signal was presented as the mean of the relative change in fluorescence intensity normalized to baseline intensity ($F - F_0/F_0$).

Mitochondrial membrane potential, ROS concentration, and mitochondrial ETC activity assay

Mitochondrial membrane potential, ROS concentration, and activities of mitochondrial ETC I, II, and V were measured using commercially available kits (C2006 and S0033S, Beyotime, China; BC0515, BC3235, and BC1445, Solarbio, China), according to the manufacturer's instructions.

Mitochondrial respiration assay

The OCR of transfected myoblasts were measured using a Seahorse XF Cell Mito Stress Test Kit (103015, Agilent Technologies, CA, USA) and by a Seahorse XF96 Extracellular Flux Analyzer (Agilent Technologies) following the manufacturer's protocol.

Statistical analysis

In this study, all experiments were repeated at least three times, and results were representative of mean ± SEM. Where applicable, the statistical significance of the data was tested using an independent-sample t test or ANOVA followed by Dunnett's test. The types of tests and the p values, when applicable, are indicated in the figure legends.

SUPPLEMENTAL INFORMATION

Supplemental information can be found online at https://doi.org/10.1016/j.omtn.2021.12.004.

ACKNOWLEDGMENTS

This work was supported by the Natural Scientific Foundation of China (U1901206, 31802051, and 31761143014), Local Innovative and Research Teams Project of Guangdong Province (2019BT02N630), Ten-Thousand Talents Program (W03020593), and China Agricultural Research System (CARS-41-G03).

AUTHOR CONTRIBUTIONS

Q.N., X.Z., and H.L. conceived and designed the study. B.C. and M.M. performed the experiments, interpreted the data, and wrote the paper. J.Z., Z.W., S.K., and Z.Z. performed the experiments. L.L., J.Z., J.L., and Y.W. interpreted the data. All authors read and approved the final manuscript.

DECLARATION OF INTERESTS

The authors declare no competing interests.

REFERENCES

1. Rai, M., and Demontis, F. (2016). Systemic nutrient and stress signaling via myokines and myometabolites. Annu. Rev. Physiol. *78*, 85–107.
2. Ibrahim, A., Neinast, M., and Arany, Z.P. (2017). Myobolites: muscle-derived metabolites with paracrine and systemic effects. Curr. Opin. Pharmacol. *34*, 15–20.
3. Janssen, I., Heymsfield, S.B., Wang, Z.M., and Ross, R. (2000). Skeletal muscle mass and distribution in 468 men and women aged 18-88 yr. J. Appl. Physiol. *89*, 81–88.
4. Bowen, T.S., Schuler, G., and Adams, V. (2015). Skeletal muscle wasting in cachexia and sarcopenia: molecular pathophysiology and impact of exercise training. J. Cachexia Sarcopenia Muscle *6*, 197–207.
5. Godfrey, R., and Quinlivan, R. (2016). Skeletal muscle disorders of glycogenolysis and glycolysis. Nat. Rev. Neurol. *12*, 393–402.
6. Sartorelli, V., and Fulco, M. (2004). Molecular and cellular determinants of skeletal muscle atrophy and hypertrophy. Sci. STKE *2004*, e11.
7. Jagoe, R.T., and Goldberg, A.L. (2001). What do we really know about the ubiquitin-proteasome pathway in muscle atrophy? Curr. Opin. Clin. Nutr. Metab. Care *4*, 183–190.
8. Thomson, D.M. (2018). The role of AMPK in the regulation of skeletal muscle size, hypertrophy, and regeneration. Int. J. Mol. Sci. *19*, 3125.
9. Zanou, N., and Gailly, P. (2013). Skeletal muscle hypertrophy and regeneration: interplay between the myogenic regulatory factors (MRFs) and insulin-like growth factors (IGFs) pathways. Cell. Mol. Life Sci. *70*, 4117–4130.
10. Blaauw, B., Schiaffino, S., and Reggiani, C. (2013). Mechanisms modulating skeletal muscle phenotype. Compr. Physiol. *3*, 1645–1687.
11. Yamada, Y., Namba, K., and Fujii, T. (2020). Cardiac muscle thin filament structures reveal calcium regulatory mechanism. Nat. Commun. *11*, 153.
12. Borowiec, A.S., Bidaux, G., Pigat, N., Goffin, V., Bernichtein, S., and Capiod, T. (2014). Calcium channels, external calcium concentration and cell proliferation. Eur. J. Pharmacol. *739*, 19–25.
13. Wang, S.F., Liu, L.F., Wu, M.Y., Cai, C.Z., Su, H., Tan, J., Lu, J.H., and Li, M. (2017). Baicalein prevents 6-OHDA/ascorbic acid-induced calcium-dependent dopaminergic neuronal cell death. Sci. Rep. *7*, 8398.
14. Berridge, M.J. (2016). The inositol trisphosphate/calcium signaling pathway in health and disease. Physiol. Rev. *96*, 1261–1296.
15. Lasa-Elgarresta, J., Mosqueira-Martin, L., Naldaiz-Gastesi, N., Saenz, A., Lopez, D.M.A., and Vallejo-Illarramendi, A. (2019). Calcium mechanisms in limb-girdle muscular dystrophy with CAPN3 mutations. Int. J. Mol. Sci. *20*, 4548.
16. Vallejo-Illarramendi, A., Toral-Ojeda, I., Aldanondo, G., and Lopez, D.M.A. (2014). Dysregulation of calcium homeostasis in muscular dystrophies. Expert Rev. Mol. Med. *16*, e16.
17. Hadrevi, J., Barbe, M.F., Ortenblad, N., Frandsen, U., Boyle, E., Lazar, S., Sjogaard, G., and Sogaard, K. (2019). Calcium fluxes in work-related muscle disorder: implications from a rat model. Biomed. Res. Int. *2019*, 5040818.
18. Bohnert, K.R., McMillan, J.D., and Kumar, A. (2018). Emerging roles of ER stress and unfolded protein response pathways in skeletal muscle health and disease. J. Cell. Physiol. *233*, 67–78.
19. Stammers, A.N., Susser, S.E., Hamm, N.C., Hlynsky, M.W., Kimber, D.E., Kehler, D.S., and Duhamel, T.A. (2015). The regulation of sarco(endo)plasmic reticulum calcium-ATPases (SERCA). Can. J. Physiol. Pharmacol. *93*, 843–854.
20. Leem, J., and Koh, E.H. (2012). Interaction between mitochondria and the endoplasmic reticulum: implications for the pathogenesis of type 2 diabetes mellitus. Exp. Diabetes Res. *2012*, 242984.

21. Rieusset, J. (2011). Mitochondria and endoplasmic reticulum: mitochondria-endoplasmic reticulum interplay in type 2 diabetes pathophysiology. Int. J. Biochem. Cell Biol. *43*, 1257–1262.

22. Lim, J.H., Lee, H.J., Ho, J.M., and Song, J. (2009). Coupling mitochondrial dysfunction to endoplasmic reticulum stress response: a molecular mechanism leading to hepatic insulin resistance. Cell Signal. *21*, 169–177.

23. Lee, J.T. (2012). Epigenetic regulation by long noncoding RNAs. Science *338*, 1435–1439.

24. Cabili, M.N., Trapnell, C., Goff, L., Koziol, M., Tazon-Vega, B., Regev, A., and Rinn, J.L. (2011). Integrative annotation of human large intergenic noncoding RNAs reveals global properties and specific subclasses. Genes Dev. *25*, 1915–1927.

25. Djebali, S., Davis, C.A., Merkel, A., Dobin, A., Lassmann, T., Mortazavi, A., Tanzer, A., Lagarde, J., Lin, W., Schlesinger, F., et al. (2012). Landscape of transcription in human cells. Nature *489*, 101–108.

26. Lu, L., Sun, K., Chen, X., Zhao, Y., Wang, L., Zhou, L., Sun, H., and Wang, H. (2013). Genome-wide survey by ChIP-seq reveals YY1 regulation of lincRNAs in skeletal myogenesis. EMBO J. *32*, 2575–2588.

27. Wang, L., Zhao, Y., Bao, X., Zhu, X., Kwok, Y.K., Sun, K., Chen, X., Huang, Y., Jauch, R., Esteban, M.A., et al. (2015). LncRNA Dum interacts with Dnmts to regulate Dppa2 expression during myogenic differentiation and muscle regeneration. Cell Res. *25*, 335–350.

28. Zhu, M., Liu, J., Xiao, J., Yang, L., Cai, M., Shen, H., Chen, X., Ma, Y., Hu, S., Wang, Z., et al. (2017). Lnc-mg is a long non-coding RNA that promotes myogenesis. Nat. Commun. *8*, 14718.

29. Ma, M., Cai, B., Jiang, L., Abdalla, B.A., Li, Z., Nie, Q., and Zhang, X. (2018). lncRNA-Six1 is a target of miR-1611 that functions as a ceRNA to regulate Six1 protein expression and fiber type Switching in chicken myogenesis. Cells *7*, 243.

30. Zhang, Z.K., Li, J., Guan, D., Liang, C., Zhuo, Z., Liu, J., Lu, A., Zhang, G., and Zhang, B.T. (2018). Long noncoding RNA lncMUMA reverses established skeletal muscle atrophy following mechanical unloading. Mol. Ther. *26*, 2669–2680.

31. Cai, B., Li, Z., Ma, M., Zhang, J., Kong, S., Abdalla, B.A., Xu, H., Jebessa, E., Zhang, X., Lawal, R.A., et al. (2021). Long noncoding RNA SMUL suppresses SMURF2 production-mediated muscle atrophy via nonsense-mediated mRNA decay. Mol. Ther. Nucleic Acids *23*, 512–526.

32. Li, Z., Cai, B., Abdalla, B.A., Zhu, X., Zheng, M., Han, P., Nie, Q., and Zhang, X. (2019). LncIRS1 controls muscle atrophy via sponging miR-15 family to activate IGF1-PI3K/AKT pathway. J. Cachexia Sarcopenia Muscle *10*, 391–410.

33. Zuo, H., and Wan, Y. (2019). Metabolic reprogramming in mitochondria of myeloid cells. Cells *9*, 5.

34. Wallace, D.C. (2012). Mitochondria and cancer. Nat. Rev. Cancer *12*, 685–698.

35. Schiaffino, S., Sandri, M., and Murgia, M. (2007). Activity-dependent signaling pathways controlling muscle diversity and plasticity. Physiology (Bethesda) *22*, 269–278.

36. Wang, T., Xu, Y.Q., Yuan, Y.X., Xu, P.W., Zhang, C., Li, F., Wang, L.N., Yin, C., Zhang, L., Cai, X.C., et al. (2019). Succinate induces skeletal muscle fiber remodeling via SUNCR1 signaling. EMBO Rep. *20*, e47892.

37. Yang, X., Brobst, D., Chan, W.S., Tse, M., Herlea-Pana, O., Ahuja, P., Bi, X., Zaw, A.M., Kwong, Z., Jia, W.H., et al. (2019). Muscle-generated BDNF is a sexually dimorphic myokine that controls metabolic flexibility. Sci. Signal. *12*, eaau1468.

38. Bassel-Duby, R., and Olson, E.N. (2006). Signaling pathways in skeletal muscle remodeling. Annu. Rev. Biochem. *75*, 19–37.

39. Schiaffino, S., and Reggiani, C. (2011). Fiber types in mammalian skeletal muscles. Physiol. Rev. *91*, 1447–1531.

40. Koutakis, P., Weiss, D.J., Miserlis, D., Shostrom, V.K., Papoutsi, E., Ha, D.M., Carpenter, L.A., McComb, R.D., Casale, G.P., and Pipinos, I.I. (2014). Oxidative damage in the gastrocnemius of patients with peripheral artery disease is myofiber type selective. Redox Biol. *2*, 921–928.

41. Li, J.B., and Goldberg, A.L. (1976). Effects of food deprivation on protein synthesis and degradation in rat skeletal muscles. Am. J. Physiol. *231*, 441–448.

42. Matsakas, A., and Patel, K. (2009). Skeletal muscle fibre plasticity in response to selected environmental and physiological stimuli. Histol. Histopathol. *24*, 611–629.

43. Joseph, A.M., Adhihetty, P.J., and Leeuwenburgh, C. (2016). Beneficial effects of exercise on age-related mitochondrial dysfunction and oxidative stress in skeletal muscle. J. Physiol. *594*, 5105–5123.

44. Braun, T., and Gautel, M. (2011). Transcriptional mechanisms regulating skeletal muscle differentiation, growth and homeostasis. Nat. Rev. Mol. Cell Biol. *12*, 349–361.

45. Saxton, R.A., and Sabatini, D.M. (2017). mTOR signaling in growth, metabolism, and disease. Cell *168*, 960–976.

46. Tan, Y., Mui, D., Toan, S., Zhu, P., Li, R., and Zhou, H. (2020). SERCA overexpression improves mitochondrial quality control and attenuates cardiac microvascular ischemia-reperfusion injury. Mol. Ther. Nucleic Acids *22*, 696–707.

47. Qaisar, R., Bhaskaran, S., Ranjit, R., Sataranatarajan, K., Premkumar, P., Huseman, K., and Van Remmen, H. (2019). Restoration of SERCA ATPase prevents oxidative stress-related muscle atrophy and weakness. Redox Biol. *20*, 68–74.

48. Gailly, P. (2002). New aspects of calcium signaling in skeletal muscle cells: implications in Duchenne muscular dystrophy. Biochim. Biophys. Acta *1600*, 38–44.

49. Rusnak, F., and Mertz, P. (2000). Calcineurin: form and function. Physiol. Rev. *80*, 1483–1521.

50. Molkentin, J.D., Lu, J.R., Antos, C.L., Markham, B., Richardson, J., Robbins, J., Grant, S.R., and Olson, E.N. (1998). A calcineurin-dependent transcriptional pathway for cardiac hypertrophy. Cell *93*, 215–228.

51. Tan, W.Q., Wang, J.X., Lin, Z.Q., Li, Y.R., Lin, Y., and Li, P.F. (2008). Novel cardiac apoptotic pathway: the dephosphorylation of apoptosis repressor with caspase recruitment domain by calcineurin. Circulation *118*, 2268–2276.

52. Reznick, R.M., Zong, H., Li, J., Morino, K., Moore, I.K., Yu, H.J., Liu, Z.X., Dong, J., Mustard, K.J., Hawley, S.A., et al. (2007). Aging-associated reductions in AMP-activated protein kinase activity and mitochondrial biogenesis. Cell Metab. *5*, 151–156.

53. He, H., Liu, X., Lv, L., Liang, H., Leng, B., Zhao, D., Zhang, Y., Du, Z., Chen, X., Li, S., et al. (2014). Calcineurin suppresses AMPK-dependent cytoprotective autophagy in cardiomyocytes under oxidative stress. Cell Death Dis. *5*, e997.

54. Wang, Y., Xie, C., Diao, Z., and Liang, B. (2017). Calcineurin antagonizes AMPK to regulate lipolysis in *Caenorhabditis elegans*. Molecules *22*, 1062.

55. Buckingham, M., and Rigby, P.W. (2014). Gene regulatory networks and transcriptional mechanisms that control myogenesis. Dev. Cell *28*, 225–238.

56. Wang, S., Jin, J., Xu, Z., and Zuo, B. (2019). Functions and regulatory mechanisms of lncRNAs in skeletal myogenesis, muscle disease and meat production. Cells *8*, 1107.

57. Luo, H., Lv, W., Tong, Q., Jin, J., Xu, Z., and Zuo, B. (2021). Functional non-coding RNA during embryonic myogenesis and postnatal muscle development and disease. Front. Cell. Dev. Biol. *9*, 628339.

58. Wang, K.C., and Chang, H.Y. (2011). Molecular mechanisms of long noncoding RNAs. Mol. Cell. *43*, 904–914.

59. Zurlo, F., Larson, K., Bogardus, C., and Ravussin, E. (1990). Skeletal muscle metabolism is a major determinant of resting energy expenditure. J. Clin. Invest. *86*, 1423–1427.

60. Boengler, K., Kosiol, M., Mayr, M., Schulz, R., and Rohrbach, S. (2017). Mitochondria and ageing: role in heart, skeletal muscle and adipose tissue. J. Cachexia Sarcopenia Muscle *8*, 349–369.

61. Boncompagni, S., Pozzer, D., Viscomi, C., Ferreiro, A., and Zito, E. (2020). Physical and functional cross talk between endo-sarcoplasmic reticulum and mitochondria in skeletal muscle. Antioxid. Redox Signal. *32*, 873–883.

62. Mizushima, N., Levine, B., Cuervo, A.M., and Klionsky, D.J. (2008). Autophagy fights disease through cellular self-digestion. Nature *451*, 1069–1075.

63. Jokl, E.J., and Blanco, G. (2016). Disrupted autophagy undermines skeletal muscle adaptation and integrity. Mamm. Genome *27*, 525–537.

64. Masiero, E., Agatea, L., Mammucari, C., Blaauw, B., Loro, E., Komatsu, M., Metzger, D., Reggiani, C., Schiaffino, S., and Sandri, M. (2009). Autophagy is required to maintain muscle mass. Cell Metab. *10*, 507–515.

65. Shen, S., Liao, Q., Liu, J., Pan, R., Lee, S.M., and Lin, L. (2019). Myricanol rescues dexamethasone-induced muscle dysfunction via a sirtuin 1-dependent mechanism. J. Cachexia Sarcopenia Muscle *10*, 429–444.

66. Cai, B., Ma, M., Chen, B., Li, Z., Abdalla, B.A., Nie, Q., and Zhang, X. (2018). MiR-16-5p targets SESN1 to regulate the p53 signaling pathway, affecting myoblast proliferation and apoptosis, and is involved in myoblast differentiation. Cell Death Dis. *9*, 367.

67. Ding, L., Yang, X., Tian, H., Liang, J., Zhang, F., Wang, G., Wang, Y., Ding, M., Shui, G., and Huang, X. (2018). Seipin regulates lipid homeostasis by ensuring calcium-dependent mitochondrial metabolism. EMBO J. *37*, e97572.